Pergamon

Int. J. Mach. Tools Manufact. Vol. 37, No. 5, pp. 687–707, 1997

0890-6955/97$17.00 + .00

S0890-6955(96)00006-5

MODELING AND ANALYSIS OF NONLINEAR GUIDEWAY FOR DOUBLE-BALL BAR (DBB) MEASUREMENT AND DIAGNOSIS

J.-M. LAI,† J.-S. LIAO† and W.-H. CHIENG†‡

(*Received* 25 *September* 1995)

Abstract—The purpose of this paper is to study nonlinear geometric errors in multi-axis machine tools. A general mathematical model for guideway systems that can be applied to high-precision machine tools such as CNC lathes is introduced. Using this model, most nonlinear error sources in the guideway systems can be diagnosed by measuring the contouring error using a double-ball bar (DBB). Diagnostic software has been developed to identify system parameters based on the least-squares estimation method. Inputting two or three contouring errors pattern data into this software enables parameters to be identified quickly, based on the nonlinear model. © 1997 Published by Elsevier Science Ltd. All rights reserved.

1. INTRODUCTION

The relative positioning accuracy of a multi-axis machine tool can be affected not only by the leadscrew pitch or straightness, but also by the orientation phenomena such as Abbe errors [1] or by general geometric characteristics. Besides the geometric characteristics, the dynamic characteristics which vary according to feed rate can affect the quality of contouring accuracy during the two- or three-dimensional contouring machining. Mismatches between servo-loop parameters [2, 3], such as current-loop gain, velocity-loop gain and position-loop gain, can also directly affect the contouring accuracy.

Theoretical methods for analyzing and diagnosing motion errors from the pattern of contouring errors found using the DBB test equipment, as shown in Fig. 1, have been discussed in several research reports. Knapp [4] studied the relationship between the contouring error patterns, plotted in polar coordinates, and the machine's motion error. However, his method for diagnosing motion error is too rough and the magnitude of the motion error cannot be calculated. Kunzmann *et al.* [5] considered the characteristic of a two-dimensional matrix including the squareness and longitudinal parameters to formulate a motion-error description. This formulation only interprets the geometry of the longitudinal and squareness errors. Kakino *et al.* [6] described various motion errors using error vectors. However, the formulation they developed cannot systematically describe the various contouring errors, and their characteristic patterns of motion errors have not been fully applied to the purpose of various motion errors.

Recently, Jeng *et al.* [7] established mathematical models using linear modelling and second-order models. Their method was found to be capable of resolving many error parameters such as center-offset errors, roll–yaw–pitch errors and servo-gain mismatches. However, this error model cannot match the high precision requirements of general guideway systems, such as the straightness requirements for a lathe machine.

2. COORDINATE SYSTEMS

This paper is focussed on the geometric errors in multi-axis machine tools. We establish a general mathematical model, called the high-order guideway coordinate system, to satisfy high-precision requirements. We also derive diagnostic procedures for motion-error sources based on two or three pattern data obtained from a circle-contouring test. Accord-

†Department of Mechanical Engineering, National Chiao-Tung University, 1001 Ta-Hsueh Road, Hsinchu, 30049, Taiwan, Republic of China
‡Author to whom correspondence should be addressed.

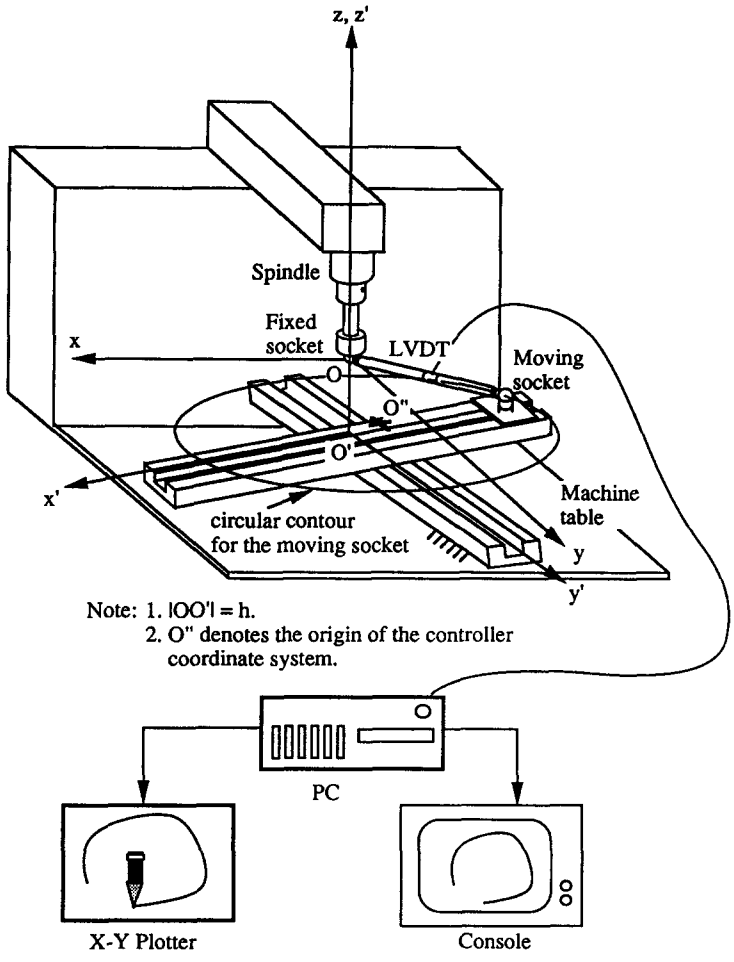

Fig. 1. Configuration of the DBB test experiment.

ing to this diagnostic method, nonlinear guideway errors in high-precision NC machines such as lathes can be accurately diagnosed.

In this paper, we assume guideways (X, Y, Z) are deflected corresponding to arbitrary roll–yaw–pitch motion errors. Using the Taylor expansion, we derive nth-order equations to match the true roll–yaw–pitch errors. For lathes and grinding machines that require accurate straightness parameters, the general model can be used to precisely isolate sources of motion errors. In formulating the motion errors in NC tools, it was assumed that the X guideway was always mounted on top of the Y guideway, Fig. 2(a) shows a typical machining center, and Fig. 2(b) shows roll–yaw–pitch angles. In the following description, the superscripts (′) and (″) are used for guideway coordinates and control coordinates, respectively. According to the nonlinearity modelling shown in Fig. 3, the contouring error ΔL may be obtained through a sequence of coordinate transformations.

3. *X*-GUIDEWAY ERROR

3.1. x- *and* y-*yaw error (guideway bending on the* x–y *plane)*

According to Fig. 4, the x-yaw error may be formulated as follows:

$$y_{x-\text{yaw}} = \sum_{k=0}^{n} a_k x^k, \tag{1}$$

where the x-yaw angle is a function of the x coordinate:

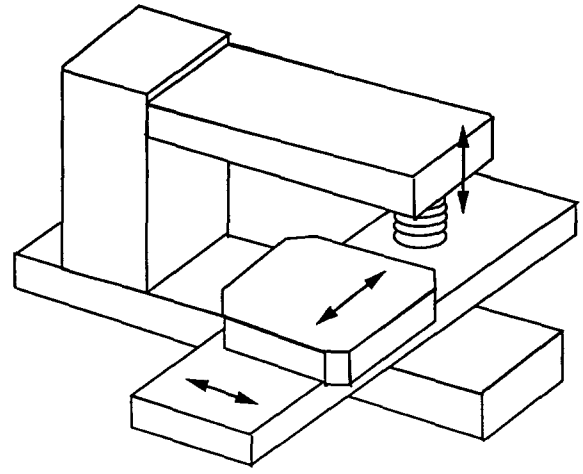

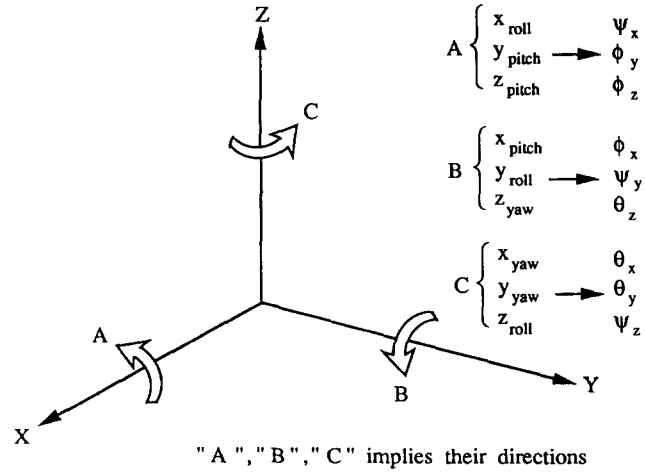

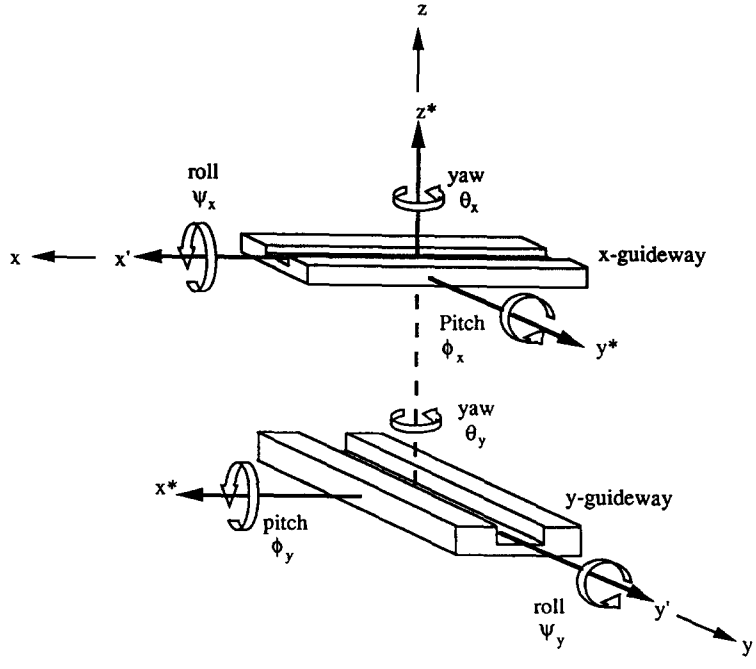

Fig. 2. (a) Typical machining center—*X*-guideway is mounted on the top of the *Y*-guideway and roll, yaw and pitch directions. (b) The roll, pitch and yaw angles of the guideways.

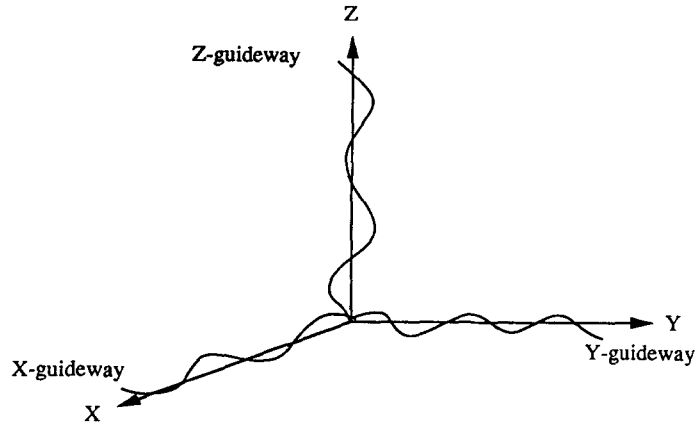

Fig. 3. *X*-, *Y*- and *Z*-guideway relative to absolute coordinates for *n*-order nonlinearity modeling.

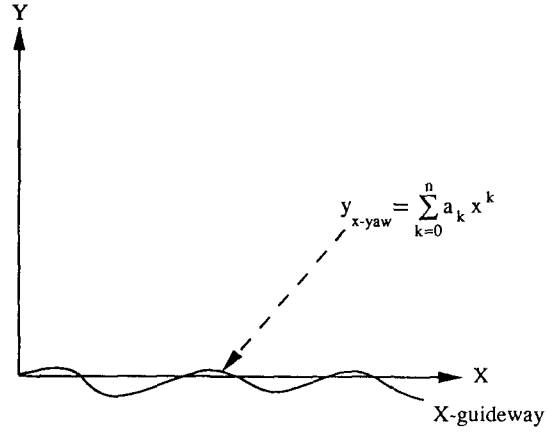

Fig. 4. *X*-guideway relative to absolute coordinates for *x*-yaw error.

$$\theta_x = \tan^{-1}\frac{dy}{dx} = \tan^{-1}\sum_{k=0}^{n} a_k \cdot k \cdot x^{k-1} \cong \sum_{k=0}^{n} a_k \cdot k \cdot x^{k-1} \text{ for small } a_k\text{s}.$$

According to Fig. 5, the *y*-yaw error may be formulated as follows:

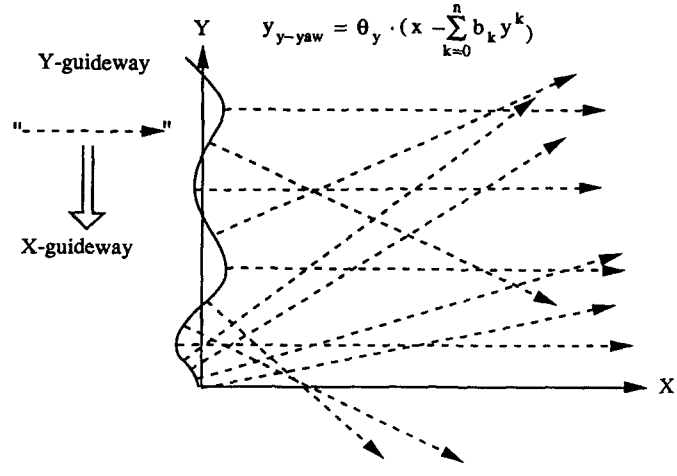

Fig. 5. *X*-guideway relative to absolute coordinates for *y*-yaw error.

$$x_{y-\text{yaw}} = \sum_{k=0}^{n} b_k y^k,$$

where the y-yaw angle is a function of the y coordinate:

$$\theta_y = -\tan^{-1}\frac{dx}{dy} = -\tan^{-1}\sum_{k=0}^{n} b_k \cdot k \cdot y^{k-1}.$$

The X-guideway is yawed and yields a squareness error of

$$y_{y-\text{yaw}} = \theta_y \cdot (x - \sum_{k=0}^{n} b_k y^k). \tag{2}$$

From Equations (1)–(2) we obtain the error sum:

$$y_{x-,\ y-\text{yaw}} = \sum_{k=0}^{n} a_k x^k + \theta_y \cdot (x - \sum_{k=0}^{n} b_k y^k).$$

Let

$$x_{x-,\ y-\text{yaw}} = f(\theta_x),$$

we then obtain

$$y_{x-\ ,y-\text{yaw}} = \sum_{k=0}^{n} a_k f^k(\theta_x) + \theta_y \cdot (f(\theta_x) - \sum_{k=0}^{n} b_k y^k), \tag{3}$$

where a_k and b_k are error parameters, $f(\Theta_x)$ denotes the x-axis world coordinate.

3.2. x-*Pitch error (*X *guideway bending around the* z*-axis) and* y*-roll error (*Y *guideway twist)*

According to Fig. 6, the x-pitch error may be formulated as follows:

$$z_{x-\text{pitch}} = \sum_{k=0}^{n} d_k x^k, \tag{4}$$

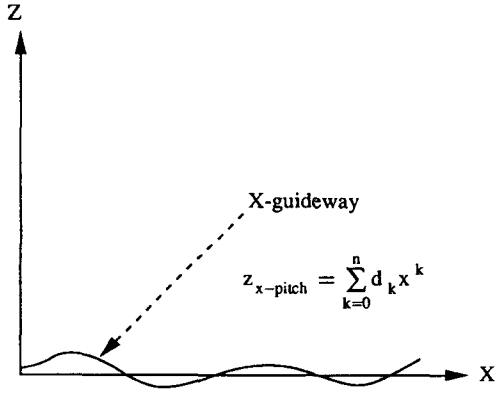

Fig. 6. X-guideway relative to absolute coordinates for x-pitch error.

where the x-pitch angle is a function of the x coordinate:

$$\phi_x = \tan^{-1} \sum_{k=0}^{n} -k \cdot d_k \cdot x^{k-1} \cong - \sum_{k=0}^{n} k \cdot d_k \cdot x^{k-1} \text{ for small } d_k\text{s}.$$

According to Fig. 7, the y-roll error may be formulated as follows:

$$\psi_y = \tan^{-1} \sum_{k=0}^{n-1} c_k y^k$$

and

$$z_{y-\text{roll}} = -x \tan\psi_y = -x \cdot \sum_{k=0}^{n-1} c_k y^k. \tag{5}$$

From Equations (4) and (5), we obtain the error sum:

$$z_{x-\text{pitch},\ y-\text{yaw}} = -x \cdot \sum_{k=0}^{n-1} c_k y^k + \sum_{k=o}^{n} d_k x^k.$$

Let

$$x_{x-\text{pitch},\ y-\text{roll}} = g(\phi_x),$$

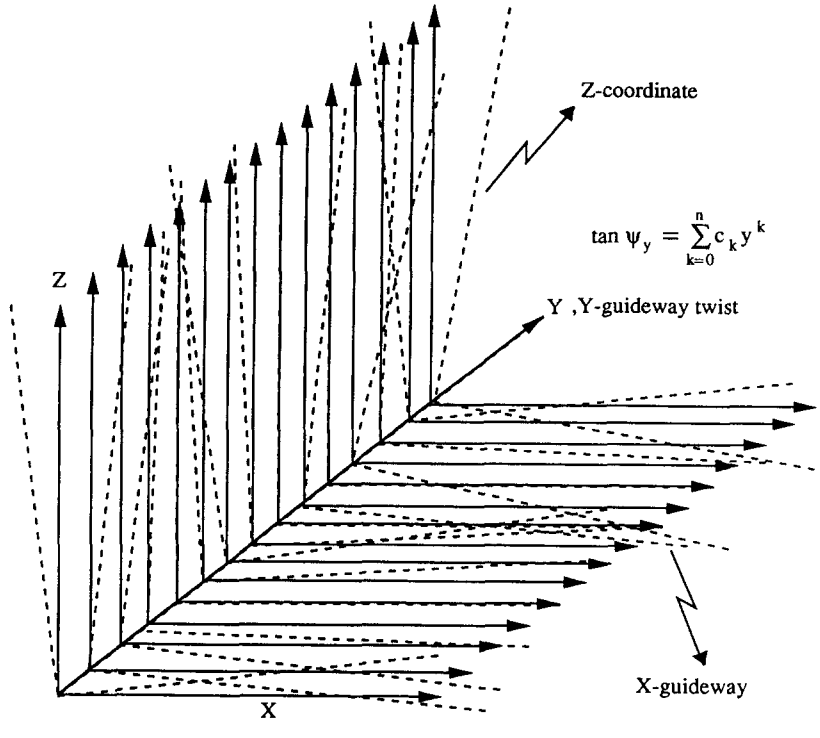

$$z_{y-\text{roll}} = x \cdot \tan \psi_y$$

Fig. 7. X-guideway relative to absolute coordinates for y-roll error.

we then obtain

$$z_{x-\text{pitch, } y-\text{roll}} = -g(\phi_x)\cdot\psi_y + \sum_{k=o}^{n} d_k\cdot g^k(\phi_x),$$

where c_k and d_k are error parameters, and $g(\phi_x)$ denotes the x-axis world coordinate.

4. Y-GUIDEWAY ERROR

4.1. y-*Yaw error (Y-guideway bending on the* x–y *plane)*

According to Fig. 8, the y-yaw error may be formulated as follows:

$$x = \sum_{k=0}^{n} b_k y^k,$$

where the y-yaw angle is a function of the y coordinate:

$$\theta_y = -\tan^{-1}\frac{dx}{dy} = -\tan^{-1}\sum_{k=0}^{n} b_k\cdot k\cdot y^{k-1}.$$

Let

$$y_{y-\text{yaw}} = h(\theta_y),$$

we then obtain

$$x_{y-\text{yaw}} = \sum_{k=0}^{n} b_k\cdot h^k(\theta_y), \tag{6}$$

where b_k is an error parameter and $h(\Theta_y)$ denotes the y-axis world coordinate.

4.2. y-*Pitch error (Y-guideway bending around the* z*-axis)*

According to Fig. 9, the y-pitch error may be formulated as follows:

$$z = \sum_{k=0}^{n} e_k y^k,$$

where the y-pitch angle is a function of the y coordinate:

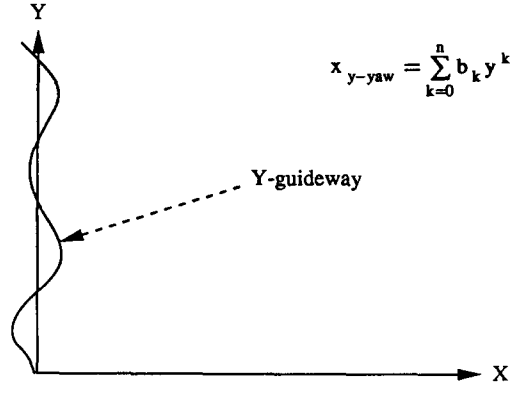

Fig. 8. *Y*-guideway relative to absolute coordinates for y-yaw error.

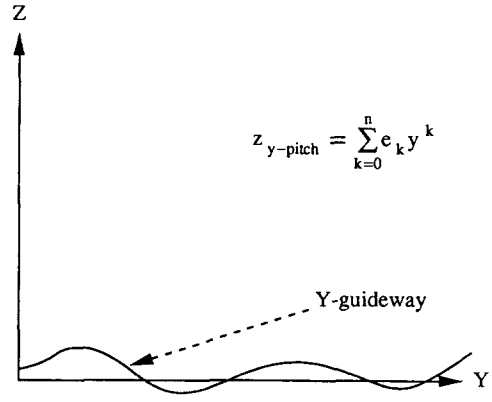

Fig. 9. *Y*-guideway relative to absolute coordinates for *y*-pitch error.

$$\phi_y = \tan^{-1}\frac{dz}{dy} = \tan^{-1}\sum_{k=0}^{n} e_k \cdot k \cdot y^{k-1}.$$

Let

$$y_{y-\text{pitch}} = l(\phi_y),$$

we then obtain

$$z_{y-\text{pitch}} = \sum_{k=0}^{n} e_k \cdot l^k(\phi_y), \tag{7}$$

where b_k is an error parameter and $l(\Theta_y)$ denotes the *y*-axis world coordinate.

5. Z-GUIDEWAY ERROR

5.1. *z-Yaw error (Z-guideway bending about* x*-axis)*

According to Fig. 10, the *z*-yaw error may be formulated as follows:

$$x = \sum_{k=0}^{n} v_k z^k,$$

where the *z*-yaw angle is a function of the *z* coordinate:

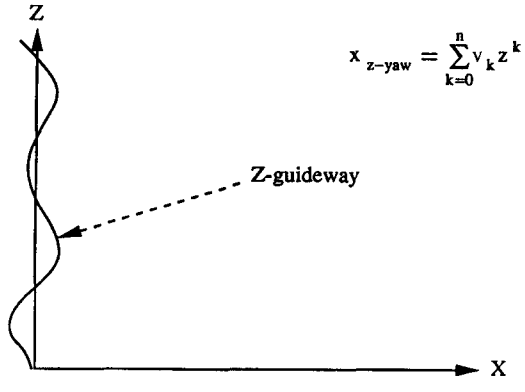

Fig. 10. *Z*-guideway relative to absolute coordinates for *z*-yaw error.

$$\theta_z = \tan^{-1}\frac{dx}{dz} = \tan^{-1}\sum_{k=0}^{n} v_k \cdot k \cdot z^{k-1}.$$

Let

$$z_{z-\text{yaw}} = m(\theta_z),$$

we then obtain

$$x_{z-\text{yaw}} = \sum_{k=0}^{n} v_k \cdot m^k(\theta_z). \tag{8}$$

5.2. z-*Pitch error (Z-guideway bending about* y-*axis)*

According to Fig. 11, the z-pitch error may be formulated as follows:

$$y = \sum_{k=0}^{n} s_k z^k,$$

where the z-pitch angle is a function of the z coordinate:

$$\phi_z = -\tan^{-1}\frac{dy}{dz} = -\tan^{-1}\sum_{k=0}^{n} s_k \cdot k \cdot z^{k-1}.$$

Let

$$z_{z-\text{pitch}} = P(\theta_z),$$

we then obtain

$$y_{z-\text{pitch}} = \sum_{k=0}^{n} s_k \cdot p^k(\phi_z), \tag{9}$$

where v_k and s_k are error parameters, and $m(\Theta_z)$ and $p(\phi_z)$ denote the z-axis world coordinates.

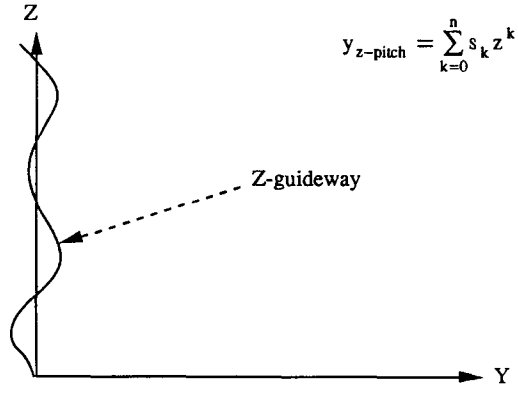

Fig. 11. Z-guideway relative to absolute coordinates for z-pitch error.

6. *X*-GUIDEWAY COORDINATE

According to the *X*-guideway deformations in Equations (3)–(5), any point in the CNC work zone $(x', y', z')_{\text{guideway-coordinates}}$ can be transformed into world coordinates $(x, y, z)_{\text{world-coordinates}}$ by the following transformation [8]:

$$\begin{bmatrix} x \\ y \\ z \\ 1 \end{bmatrix}_{\text{world-coordinates}} = \begin{bmatrix} 1 & -(\theta_x + \theta_y) & (\phi_x + \psi_y) & 0 \\ 0 & 1 & 0 & y_{x-,\ y-\text{yaw}} \\ 0 & 0 & 1 & z_{x-\text{pitch},y-\text{roll}} \\ 0 & 0 & 0 & 1 \end{bmatrix} \begin{bmatrix} x' \\ y' \\ z' \\ 1 \end{bmatrix}_{\text{guideway-coordinates}} \tag{10}$$

$$\Rightarrow \begin{cases} x = x' - y' \cdot (\theta_x + \theta_y) + z' \cdot (\phi_x + \psi_y) \\ y = y' + \sum_{k=0}^{n} a_k \cdot f^k(\theta_x) + \theta_y \cdot (f(\theta_x) - \sum_{k=0}^{n} b_k y^k). \\ z = z' - g(\phi_x) \cdot \psi_y + \sum_{k=1}^{n} d_k \cdot g^k(\phi_x) \end{cases}$$

7. *Y*-GUIDEWAY COORDINATE

According to the *Y*-guideway deformations in Equations (6) and (7), any point in the CNC work zone $(x', y', z')_{\text{guideway-coordinates}}$ can be transformed into world coordinates $(x, y, z)_{\text{world-coordinates}}$ by the following transformation:

$$\begin{bmatrix} x \\ y \\ z \\ 1 \end{bmatrix}_{\text{world-coordinates}} = \begin{bmatrix} 1 & 0 & 0 & x_{y-\text{yaw}} \\ \theta_y & 1 & -\phi_y & 0 \\ 0 & 0 & 1 & z_{y-\text{pitch}} \\ 0 & 0 & 0 & 1 \end{bmatrix} \begin{bmatrix} x' \\ y' \\ z' \\ 1 \end{bmatrix}_{\text{guideway-coordinates}} \tag{11}$$

$$\Rightarrow \begin{cases} x = x' + \sum_{k=0}^{n} b_k \cdot h^k(\theta_y) \\ y = y' + x' \cdot \theta_y - z' \cdot \phi_y. \\ z = z' + \sum_{k=0}^{n} e_k \cdot l^k(\phi_y) \end{cases}$$

8. *Z*-GUIDEWAY COORDINATE

According to the *Z*-guideway deformations in Equations (8) and (9), any point in the CNC work zone $(x', y', z')_{\text{guideway-coordinates}}$ can be transformed into world coordinates $(x, y, z)_{\text{world-coordinates}}$ by the following transformation:

$$\begin{bmatrix} x \\ y \\ z \\ 1 \end{bmatrix}_{\text{world-coordinates}} = \begin{bmatrix} 1 & 0 & 0 & x_{z-\text{yaw}} \\ 0 & 1 & 0 & y_{z-\text{pitch}} \\ -\theta_z & \phi_z & 1 & 0 \\ 0 & 0 & 0 & 1 \end{bmatrix} \begin{bmatrix} x' \\ y' \\ z' \\ 1 \end{bmatrix}_{\text{guideway-coordinates}} \tag{12}$$

$$\Rightarrow \begin{cases} x = x' + \sum_{k=0}^{n} v_k \cdot m^k(\theta_z) \\ y = y' + \sum_{k=0}^{n} s_k \cdot p^k(\phi_z). \\ z = z' - x' \cdot \theta_z + y' \cdot \phi_z \end{cases}$$

9. X, Y, Z-GUIDEWAY DEFORMATION

In Equations (10)–(12), roll–yaw–pitch errors are small (several microns), and so the roll–yaw–pitch error coupling terms can be ignored. The superposition principle is applied to yield the transformation between the guideway coordinate system and the world coordinate system as follows:

$$\begin{cases} x = x' + \sum_{k=0}^{n} b_k \cdot h^k(\theta_y) + \sum_{k=0}^{n} v_k \cdot m^k(\theta_z) - y' \cdot (\theta_x + \theta_y) + z' \cdot (\phi_x + \psi_y) \\ y = y' + \sum_{k=0}^{n} a_k f^k(\theta_x) + \theta_y (f(\theta_x) - \sum_{k=0}^{n} b_k y^k) + \sum_{k=0}^{n} s_k p^k(\phi_z) + x' \cdot \theta_y - z' \cdot \phi_y. \\ z = z' - g(\phi_x) \cdot \psi_y + \sum_{k=1}^{n} d_k \cdot g^k(\phi_x) + \sum_{k=0}^{n} e_k \cdot l^k(\phi_y) - x' \cdot \theta_z + y' \cdot \phi_z \end{cases} \tag{13}$$

In the transformation between control coordinates and guideway coordinates, it is important to note that the origin, denoted by O_x, O_y, O_z, and the dimension scale, denoted by S_x, S_y, S_z, may not be identical to one another. The relationship between the control coordinates and the guideway coordinates may be expressed as follows:

$$\begin{cases} x' = S_x(O_x + x'') \\ y' = S_y(O_y + y''). \\ z' = S_z(O_z + z'') \end{cases}$$

Substituting the above equation into Equation (13), the geometrical relationship between the control coordinates and world coordinates may be obtained as follows:

$$\begin{bmatrix} x \\ y \\ z \end{bmatrix} = \begin{bmatrix} S_x(O_x + x'') + \sum_{k=0}^{n} b_k \cdot h^k(\theta_y) + \sum_{k=0}^{n} r_k \cdot m^k(\theta_z) \\ S_y(O_y + y'') + \sum_{k=0}^{n} a_k f^k(\theta_x) + \theta_y (f(\theta_x) - \sum_{k=0}^{n} b_k y^k) + \sum_{k=0}^{n} s_k p^k(\phi_z) \\ S_z(O_z + z'') - g(\phi_x) \cdot \psi_y + \sum_{k=1}^{n} d_k \cdot g^k(\phi_x) + \sum_{k=0}^{n} e_k \cdot l^k(\phi_y) \end{bmatrix}$$

$$+ \begin{bmatrix} -S_y(O_y + y'') \cdot (\theta_x - \theta_y) + S_z(O_z + z'') \cdot (\phi_x + \psi_y) \\ S_x(O_x + x'') \cdot \theta_y - S_z(O_z + z'') \cdot \phi_y \\ -S_x(O_x + x'') \cdot \theta_z + S_y(O_y + y'') \cdot \phi_z \end{bmatrix}. \tag{14}$$

10. DOUBLE-BALL BAR COORDINATE SYSTEM

In practice, the vertical projection point of the fixed socket position of the DBB, r_0^*, on the xy-plane denoted by r''_0 may not coincide with the center of circular motion. The projection point r''_0 and moving socket r''_1 in control coordinates may be written as

$$r''_0 = \begin{bmatrix} x''_0 + e_x \\ y''_0 + e_y \\ 0 \end{bmatrix}$$

and

$$r''_1 = \begin{bmatrix} x''_0 + r_0\cos\zeta \\ y''_0 + r_0\sin\zeta \\ e_z \end{bmatrix},$$

where e_x, e_y and e_z are the offset distance associated with the x-, y- and z-axis, r_0 is the radius of circular motion and ζ is the angle of circular motion, as shown in Fig. 12. Substituting the above relation into Equation (19), the variation vector $r_1 - r_0^*$ may be expressed as follows:

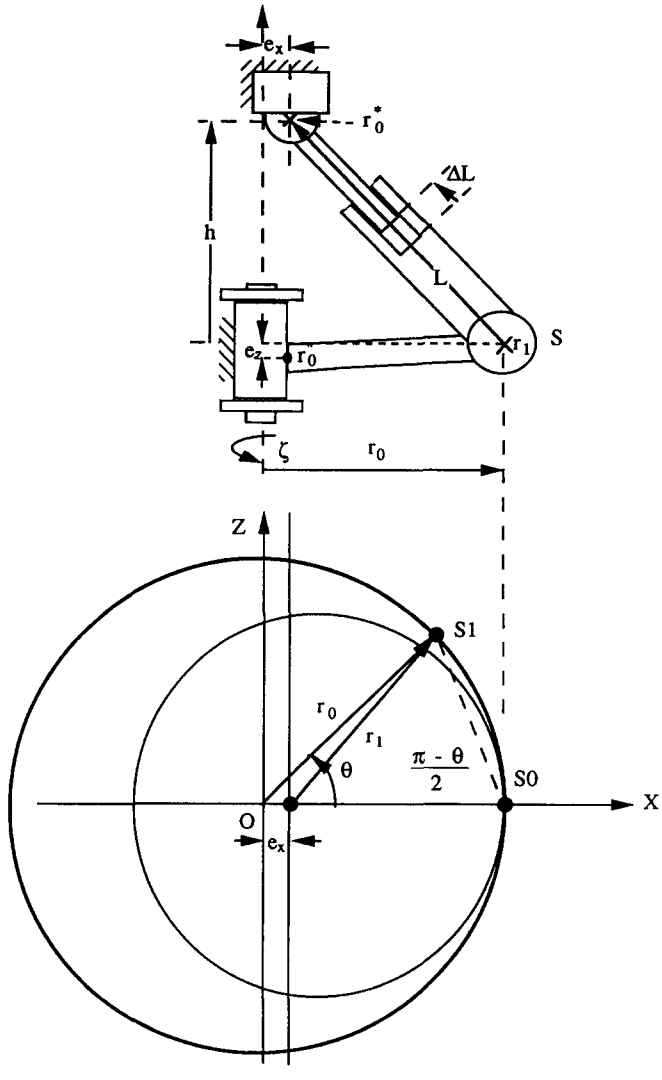

Fig. 12. The schematic diagram for offset-center error.

$$
\begin{aligned}
r_1 - r_0^* = &\begin{bmatrix} S_x(r_0\cos\zeta - e_x) \\ S_y(r_0\sin\zeta - e_y) + \sum_{k=0}^{n} a_k f^k(\theta_{x_1}) - \sum_{k=0}^{n} a_k f^k(\theta_{x_0}) + \theta_{y_1}(f(\theta_{x_1}) - \sum_{k=0}^{n} b_k y_1^k) \\ S_z(O_z + e_z - h) - g(\phi_{x_1})\cdot\psi_{y_1} + g(\phi_{x_0})\cdot\psi_{y_0} \end{bmatrix} \\
&+ \begin{bmatrix} (\sum_{k=0}^{n} b_k h^k(\theta_{y_1}) - \sum_{k=0}^{n} b_k h^k(\theta_{y_0})) + (\sum_{k=0}^{n} v_k m^k(\theta_{z_1}) - \sum_{k=0}^{n} v_k m^k(\theta_{z_0})) \\ -\theta_{y_0}(f(\theta_{x_0}) - \sum_{k=0}^{n} b_k y_0^k)) + \sum_{k=0}^{n} s_k p^k(\phi_{z_1}) - \sum_{k=0}^{n} s_k p^k(\phi_{z_0}) \\ \sum_{k=1}^{n} d_k\cdot g^k(\phi_{x_1}) - \sum_{k=1}^{n} d_k\cdot g^k(\phi_{x_0}) + \sum_{k=0}^{n} e_k\cdot l^k(\phi_{y_1}) - \sum_{k=0}^{n} e_k\cdot l^k(\phi_{y_0}) \end{bmatrix} \\
&+ \begin{bmatrix} -S_y(O_y + y_0'' + r_0\sin\zeta)\cdot(\theta_{x_1} + \theta_{y_1}) + S_y(O_y + y_0'' + e_y)\cdot(\theta_{x_0} + \theta_{y_0}) \\ S_x(O_x + x_0'' + r_0\cos\zeta)\cdot\theta_{y_1} - S_x(O_x + x_0'' + e_x)\cdot\theta_{y_0} \\ -S_x(O_x + x_0'' + r_0\cos\zeta)\cdot\theta_{z_1} + S_x(O_x + x_0'' + e_x)\cdot\theta_{z_0} \end{bmatrix} \\
&+ \begin{bmatrix} S_z(O_z + e_z)\cdot(\phi_{x_1} + \psi_{y_1}) - S_z(O_z + h)\cdot(\phi_{x_0} + \psi_{y_0}) \\ -S_z(O_z + y_0' + e_z)\cdot\phi_{y_1} + S_z(O_z + h)\cdot\phi_{y_0} \\ S_y(O_y + y_0' + r_0\sin\zeta)\cdot\phi_{z_1} - (O_y + y_0' + e_y)\cdot\phi_{z_0} \end{bmatrix},
\end{aligned} \tag{15}
$$

where the magnitudes of vectors x_0, y_0 and z_0 in world coordinates are very close to the magnitudes of vectors x'_0 and y'_0, z'_0 in guideway coordinates, and the magnitudes of vectors x_1, y_1 and z_1 in world coordinates are also very close to the magnitudes of x'_1, y'_1 and z'_1 in guideway coordinates.

11. ANALYSIS OF MOTION ERRORS FOR A THIRD-ORDER LATHE GUIDEWAY SYSTEM

Because of the high precision straightness requirements of lathes, third-order or higher recognition functions are necessary. Later, we will demonstrate a good consistency between the input simulation data and third-order motion errors.

The motion errors for third-order guideway systems can be obtained from Equation (15) and the following equation:

$$\Delta L = \| r_1 - r_0^* \| - L_0. \tag{16}$$

(1) *Center-offset error.* From Equation (16), we can derive the center offset error e_x in the x-direction as follows:

$$\Delta L = \sqrt{r_0^2 + h^2 + e_x^2 - 2e_x r_0\cos\zeta} - \sqrt{r_0^2 + h^2} \cong -\frac{e_x}{\sqrt{r_0^2 + h^2}}\cdot r_0\cos\zeta. \tag{17}$$

Similarly, the contouring error ΔL due to center-offset error e_z in the z-direction may be derived as follows:

$$\Delta L \cong -\frac{e_z}{\sqrt{L_0^2 + h^2}}\cdot L_0\sin\zeta. \tag{18}$$

(2) *Positioning scale error.* Applying Equation (16) to analyze the positioning scale error S_x in the x-direction, the contouring error ΔL may be formulated as

$$\Delta L = \sqrt{h^2 + r_0^2(\sin^2\zeta + S_x^2\cos^2\zeta)} - \sqrt{r_0^2 + h^2} \cong \frac{r_0^2(S_x - 1)}{\sqrt{r_0^2 + h^2}} \cdot \cos^2\zeta. \tag{19}$$

Similarly, the contouring error ΔL due to the position scale error S_z in the z-direction is derived as follows:

$$\Delta L \cong \frac{r_0^2(S_z - 1)}{\sqrt{r_0^2 + h^2}} \cdot \sin^2\zeta. \tag{20}$$

(3) *Straightness error.* To simplify analysis, the straightness error can be divided into three types of motion errors.

(3.1) *Yaw motion error-guideway bending on the xz-plane.* From Equation (16), the contouring error ΔL resulting from the Z-guideway bending may be expressed as follows:

$$\Delta L \approx \sqrt{r_0^2 + h^2 - 2r_0^2(b_2 r_0 \sin\zeta + 2b_3 r_0^2 \sin^2\zeta)\cos\zeta\sin\zeta} - \sqrt{r_0^2 + h^2} \cong -\frac{1}{\sqrt{r_0^2 + h^2}} \tag{21}$$
$$(r_0^3 b_2 \cdot \sin^2\zeta\cos\zeta + 2r_0^4 b_3 \cdot \sin^3\zeta\cos\zeta).$$

Similarly, the contouring error ΔL resulting from the X-guideway bending may be expressed as follows:

$$\Delta L \cong -\frac{1}{\sqrt{r_0^2 + h^2}} (r_0^3 a_2 \cdot \cos^2\zeta\sin\zeta + 2r_0^4 a_3 \cdot \cos^3\zeta\sin\zeta). \tag{22}$$

(3.2) *Pitch motion error-guideway bending about the y-axis.* From Equation (16), the contouring error ΔL for the Z-guideway bending about the y-axis may be expressed as follows:

$$\Delta L \approx \sqrt{r_0^2 + h^2 + 2e_1 h r_0 \sin\zeta + 2e_2 h r_0^2 \sin^2\zeta + 2e_3 h r_0^3 \sin^3\zeta} - \sqrt{r_0^2 + h^2} \cong \tag{23}$$
$$\frac{1}{\sqrt{r_0^2 + h^2}} (e_1 h r_0 \sin\zeta + e_2 h r_0^2 \sin^2\zeta + e_3 h r_0^3 b_3 \sin^3\zeta).$$

Similarly, the contouring error ΔL resulting from the X-guideway bending about the y-axis may be expressed as follows:

$$\Delta L \cong \frac{1}{\sqrt{r_0^2 + h^2}} \cdot (d_1 h r_0 \cos\zeta + d_2 h r_0^2 \cos^2\zeta + d_3 h r_0^3 \cos^3\zeta). \tag{24}$$

(3.3) *Roll Motion Error-Guideway Twist.* From Equation (16), the contouring error resulting from the Y-guideway twist may be expressed as follows:

$$\Delta L \approx \sqrt{r_0^2 + h^2 + 2c_0 h r_0 \cos\zeta + 2c_1 h r_0^2 \cos\zeta\sin\zeta + 2c_2 h r_0^3 \cos\zeta\sin^2\zeta} - \sqrt{r_0^2 + h^2} \cong$$
$$\frac{1}{\sqrt{r_0^2 + h^2}} (c_0 h r_0 \cos\zeta + c_1 h r_0^2 \cos\zeta\sin\zeta + c_2 h r_0^3 \cos\zeta\sin^2\zeta). \tag{25}$$

12. LEAST-SQUARE ESTIMATION FOR LINEAR FORM AND MOTION ERROR DIAGNOSIS FOR THIRD-ORDER SYSTEMS

We are considering the fitting function y, which is a linear combination of several known functions f_ks that have the following form:

$$y(\zeta) = f(\zeta;\ k_1,k_2,\ldots,k_m)$$

$$= k_1 f_1(\zeta,h) + k_2 f_2(\zeta,h) + \ldots + k_m f_m(\zeta,h), \tag{26}$$

where the dependent variable y is linear with respect to the constants k_1, k_2, k_3,..., k_m, ζ is the set of fitting data, and h denotes the height of the moving socket from the measurement table.

Letting $D_{ji}(\zeta)$ denote the ith datum of the jth pattern data set, we can derive the following equations:

$$\Sigma_r k_r \cdot \Sigma_j \Sigma_i (f_k)_i \cdot (f_r)_i = \Sigma_j \Sigma_i (f_k)_i \cdot D_{ji}, \quad k = 1,2,3,\ldots,m. \tag{27}$$

The solutions for Equation (27) are the optimum coefficients for least-squares function fitting. Then the diagnosis based on the result of the DBB circular test can be transformed into a parameter identification problem based on the least-squares method.

For third-order cases, the characteristic functions that describe the various motion errors may be found in Table 1 and are summarized as follows:

$$\begin{aligned} y = -\frac{r_0}{L_0} \{ & k_1\cos\zeta + k_2\sin\zeta - k_3 r_0 \cos^2\zeta - k_4 r_0 \sin^2\zeta \\ & + k_5 r_0^2 \cos^2\zeta\sin\zeta + k_6 r_0^3 \cos^3\zeta\sin\zeta + k_7 r_0^2 \sin^2\zeta \cos\zeta \\ & + k_8 r_0^3 \sin^3\zeta \cos\zeta + k_9 h\sin\zeta + k_{10} h r_0 \sin^2\zeta + k_{11} h r_0^2 \sin^3\zeta \\ & + k_{12} h \cos\zeta + k_{13} h r_0 \cos^2\zeta + k_{14} h r_0^2 \cos^3\zeta \\ & + k_{15} h r_0 \cos\zeta \sin\zeta + k_{16} h r_0^2 \cos\zeta \sin^2\zeta + k_{17} h r_0 \sin\zeta + k_{18} h r_0 \cos\zeta + k_{19} r_0 \\ & + k_{20} r_0^4 \cos^5\zeta + k_{21} r_0^4 \sin^5\zeta + k_{22} r_0^4 \cos^2\sin^4\zeta + k_{23} r_0^4 \cos^4\zeta \}. \end{aligned} \tag{28}$$

The different errors correspond to the coefficients of the fitting function in the following ways:

$$e_x = k_1,\ e_z = k_2,\ S_x = k_3 + 1,\ S_z = k_4 + 1,\ a_2 = k_5,\ a_3 = \frac{1}{2} k_6,\ b_2 = k_7,$$

Table 1. The characteristic functions of different motion errors

Error		Characteristic function	Harmonic order	Dependency h
Center-offset	$\Delta L_{\text{offset } x}$	$-\lambda\ e_x \cos\zeta$	1	No
	$\Delta L_{\text{offset } z}$	$-\lambda\ e_z \sin\zeta$	1	No
Position scale	ΔL_{Sx}	$\lambda\ r_0\ (S_x - 1) \cos^2\zeta$	0, 2	No
	ΔL_{Sz}	$\lambda\ r_0\ (S_z - 1) \sin^2\zeta$	0, 2	No
Yaw motion	$\Delta L_{x\text{-yaw}}$	$-\lambda r_0^2\ a_2 \cos^2\zeta \sin\zeta$	1, 3	No
		$-2\lambda r_0^3\ a_3 \cos^3\zeta \sin\zeta$	0, 2, 4	No
	$\Delta L_{z\text{-yaw}}$	$-\lambda r_0^2\ b_2 \cos\zeta \sin^2\zeta$	1, 3	No
		$-2\lambda r_0^3\ b_3 \cos\zeta \sin^3\zeta$	0, 2, 4	No
Pitch motion	$\Delta L_{x\text{-pitch}}$	$\lambda h d_2 \cos\zeta$	1	Yes
		$+\lambda h r_0 d_2 \cos^2\zeta$	0, 2	Yes
		$+\lambda h r_0^2 d_3 \cos^3\zeta$	1, 3	Yes
	$\Delta L_{z\text{-itch}}$	$\lambda h e_1 \sin\zeta$	1	Yes
		$+\lambda h r_0 e_2 \sin^2\zeta$	0, 2	Yes
		$+\lambda h r_0^2\ e_3 \sin^3\zeta$	1, 3	Yes
Roll motion	ΔL_{roll}	$\lambda h r_0 c_0 \cos\zeta$	1	Yes
		$+\lambda h r_0\ c_1 \cos\zeta \sin\zeta$	2	Yes
		$+\lambda h r_0^2\ c_2 \cos\zeta \sin^2\zeta$	1, 3	Yes

Note: $\lambda = r_0/L_0$.

$$b_3 = \frac{1}{2} k_8,\ e_1 = -k_9,\ e_2 = -k_{10},\ e_3 = -k_{11},\ d_1 + c_0 = -k_{12}$$
$$d_2 = -k_{13},\ d_3 = -k_{14},\ c_1 = -k_{15},\ c_2 = -k_{16},\ L_0 = \sqrt{r_0^2 + h^2}.$$

In order to diagnose various motion errors, two input error patterns with different heights between the sockets and different motion directions will provide sufficient information for the linearity model. However, this amount of information is not sufficient to determine nonlinearity due to the undesirable numerical truncation.

The nonlinearity model, which employs second- or third-order terms, tends to be more sensitive to numerical truncation than the linearity model. The existing numerical truncation error can practically destroy correct classifications among closed-loop gain mismatches [7]. Hence, to ensure numerical stability, a redundant set of input error patterns is necessary for nonlinearity model parametric identification. The extra input error pattern can be the same circular test experiment as the second one, but with a different tracing direction, for example counter-clockwise.

13. EXAMPLE AND DIAGNOSIS

From a purely mathematical point of view, both the height of the spindle and the radius of the circular motion should not qualitatively affect the diagnosis. However, in the practical experimental set-up the resolution of the sampling data will be reduced when either the radius of the circular motion decreases, or the height of the free socket increases. Because the input patterns produce different amounts of sampling data, the weighting between the sampling data in the least-squares method is necessary, which may affect the optimum diagnosis result. Hence, to avoid weighting problems, it is suggested that the height of the spindle be around 20 mm and the radius of circular motion be around 100 mm. In lathes, the fixed socket height should also be as small as possible.

14. SIMULATION AND EXPERIMENT

Simulations of contouring errors are specified in Table 2 and the diagnosis may be obtained from the second column of Table 3 (two patterns). A three-pattern example is shown in Table 4 and the diagnosis may be obtained from the second column of Table 5. The corresponding values of motion errors were calculated based on the least-squares method. Comparing Tables 3 and 5, we observe that the error estimations from different models are both reasonably close to the given error quantities. The roll motion, yaw motion and pitch motion parameter errors show better results in Table 5. The main factor is that the coupling terms can be resolved more effectively by combining the different error patterns, and the amount of pattern data must minimally cope with the numbers of coupling terms.

The experimental data, as shown in Fig. 13 (two patterns) and Fig. 14 (three patterns), were obtained from the experiments and detailed in Fig. 15. Diagnosis was based on experimental data, Tables 6 and 7 show the error estimation. Fig. 16 (two-pattern) and Fig. 17 (three-pattern) show the differences between the experimental pattern data and the recognition data. Comparing the experimental data with the error-estimation data in Figs 16 and 17, we find that the recognition results from the three-pattern data diagnosis are better measured as variance than the recognition results from the two-pattern data diagnosis.

Table 2. Setting in software simulation for the input error pattern generation.

Input error pattern	Height (mm)	Radius (mm)	Tracing direction
Number 2	31.225	95.00	CW
Number 3	0.000	100.00	CCW

Table 3. Diagnosis from the simulation data based on the nonlinear (third-order) models, respectively

Error causes	Given	Nonlinear model
e_x (μm)	−2.0	−1.95678
e_z (μm)	−3.0	−3.06134
Backlash x (μm)	1.0	0.9979
Backlash y (μm)	2.0	1.9983
S_x	0.99999	0.99999
S_y	1.00001	1.00001
Misalignment angle x	0.0380	0.0332
Misalignment angle y	0.0350	0.0302
Mismatch phase angle	0	0.0002
a_1 (squareness error)	3.0×10^{-4} (rad)	3.36×10^{-5} (rad)
a_2	2.2500×10^{-7}	2.2348×10^{-7}
a_3	-5.00×10^{-9}	-8.38×10^{-9}
b_2	2.5000×10^{-7}	2.5108×10^{-7}
b_3	5.00×10^{-9}	8.38×10^{-9}
c_0+d_1	2.0×10^{-4}	2.6×10^{-4}
c_1	2.500×10^{-6}	3.339×10^{-6}
c_2	-5.000×10^{-8}	-3.975×10^{-8}
d_2	6.0000×10^{-7}	7.0514×10^{-7}
d_3	-1.1×10^{-8}	-3×10^{-11}
e_1	1.0×10^{-6}	1.6×10^{-6}
e_2	1.50000×10^{-6}	1.38841×10^{-6}
e_3	-1.500×10^{-8}	-1.389×10^{-8}

Table 4. Data setting in software simulation for the input error pattern generation

Input error pattern	Height (mm)	Radius (mm)	Tracing direction
Number 1	31.225	95.00	CCW
Number 2	31.225	95.00	CW
Number 3	0.00	100.00	CCW

Table 5. Diagnosis from the simulation data based on the nonlinear (third-order) models, respectively

Error causes	Given	Nonlinear model
e_x (μm)	−2.0	−2.01348
e_z (μm)	−3.0	−2.99455
Backlash x (μm)	1.0	1.01230
Backlash y (μm)	2.0	1.95340
S_x	0.99999	0.99999
S_y	1.00001	1.00001
Misalignment angle x	0.0380	0.0391
Misalignment angle y	0.0350	0.0358
Mismatch phase angle	0	0.0007
a_1 (squareness error)	3.00×10^{-4} (rad)	3.18×10^{-4} (rad)
a_2	2.2500×10^{-7}	2.2346×10^{-7}
a_3	-5.00×10^{-9}	-5.25×10^{-9}
b_2	2.5000×10^{-7}	2.5108×10^{-7}
b_3	5.00×10^{-9}	5.25×10^{-9}
c_0+d_1	2.0000×10^{-4}	1.9566×10^{-4}
c_1	2.50000×10^{-6}	2.46851×10^{-6}
c_2	-5.000×10^{-8}	-4.637×10^{-8}
d_2	6.0000×10^{-7}	6.5281×10^{-7}
d_3	-1.10×10^{-8}	-6.97×10^{-9}
e_1	1.000×10^{-4}	1.056×10^{-4}
e_2	1.50000×10^{-6}	1.44459×10^{-6}
e_3	-1.500×10^{-8}	-1.445×10^{-8}

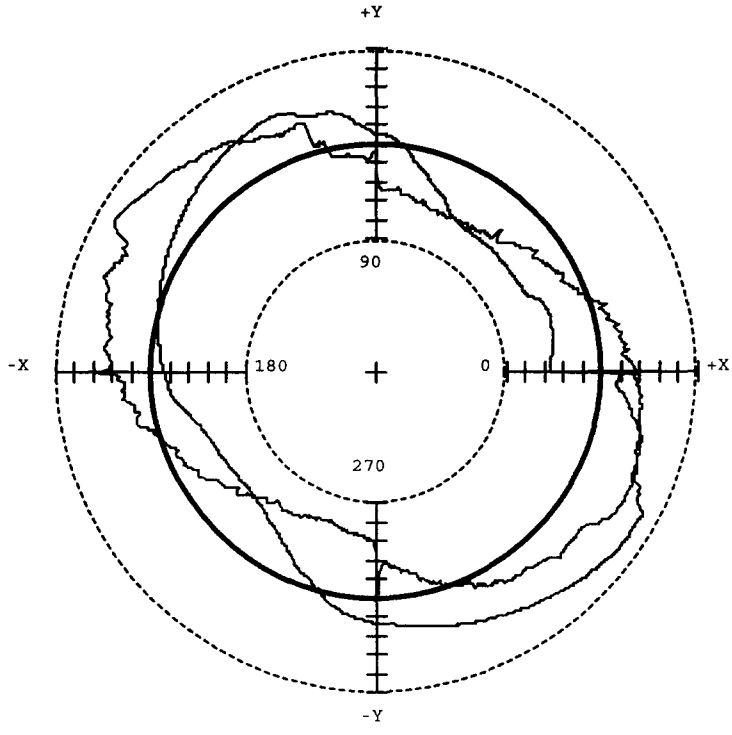

Fig. 13. The experimental pattern data—two patterns.

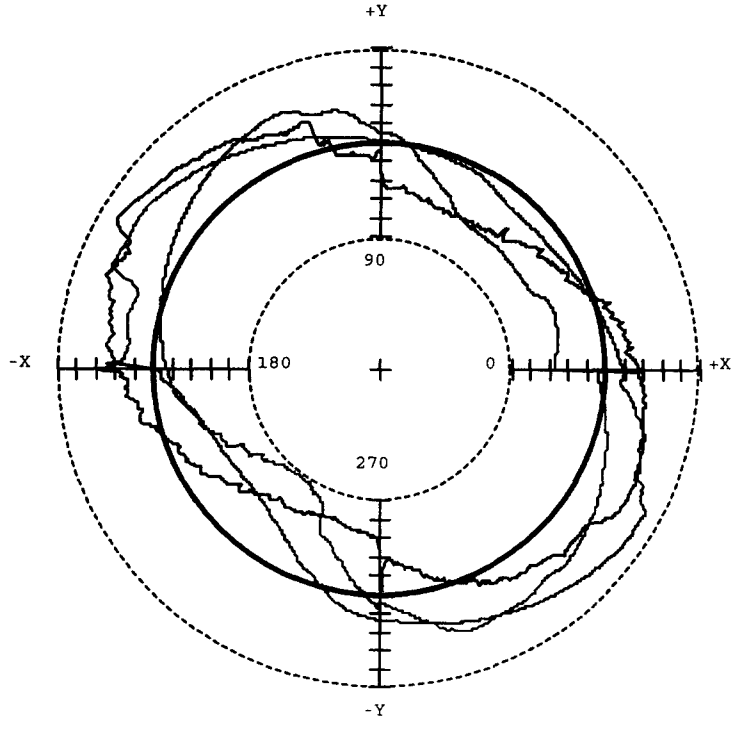

Fig. 14. The experimental pattern data—three patterns.

15. CONCLUSION

We have introduced a general, mathematical model for machine tool guideway systems. This model is applicable to real guideway systems in machine tools and can be used to analyze high-precision machine tools. We can easily convert the general model to a simpli-

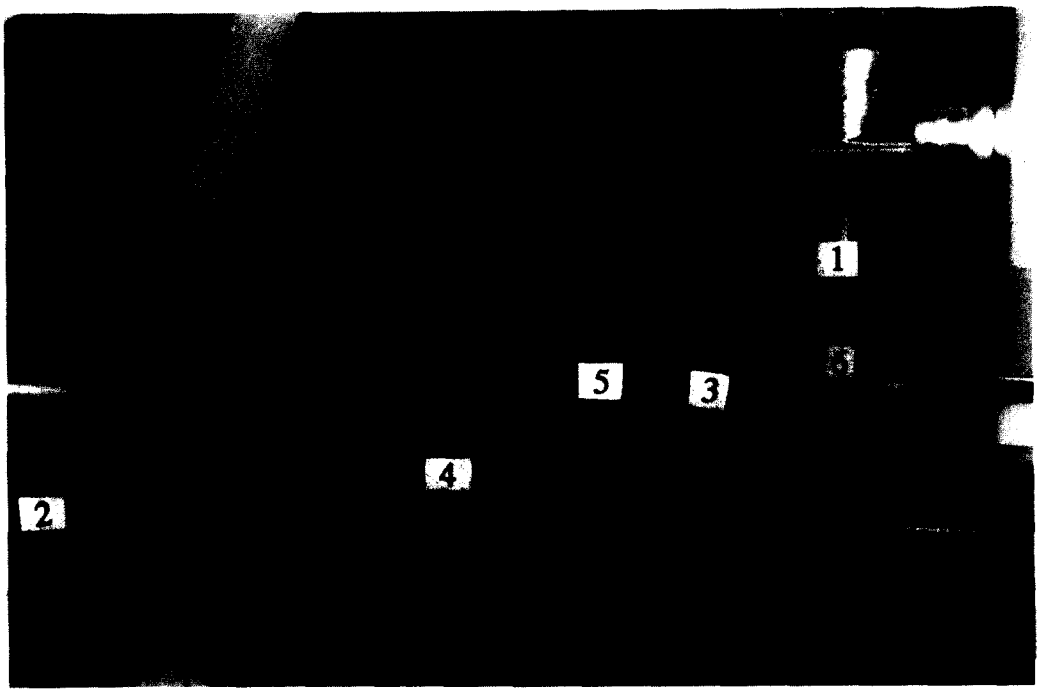

Fig. 15. The experimental equipment.

Table 6. Data setting in software simulation for the experiment pattern generation

Experiment error patterns	Height (mm)	Radius (mm)	Tracing direction
Number 1	43.589	90.00	CW
Number 2	31.225	95.00	CCW

Table 7. Diagnosis from the experiment data based on the nonlinear (third-order) models, respectively

Error causes	Recognition results
e_x (μm)	14.6321 (no. 1) 7.73738 (no. 2)
e_z (μm)	15.0370 (no. 1) −40.4931 (no. 2)
Backlash x (μm)	3.7557
Backlash y (μm)	3.2319
S_x	1.0003
S_y	0.999185
Misalignment angle x	0.0098
Misalignment angle y	0.0296
Mismatch phase angle	0.0002
a_1 (squareness error)	-2.52033×10^{-2} (rad)
a_2	-1.76620×10^{-6}
a_3	5.94×10^{-9}
b_2	2.25654×10^{-6}
b_3	7.09×10^{-9}
c_0+d_1	4.4883831×10^{-4}
c_1	2.936200×10^{-5}
c_2	-8.6910×10^{-7}
d_2	2.751047×10^{-5}
d_3	-8.7818×10^{-7}
e_1	78715373×10^{-4}
e_2	1.1005×10^{-7}
e_3	-1.1589×10^{-7}

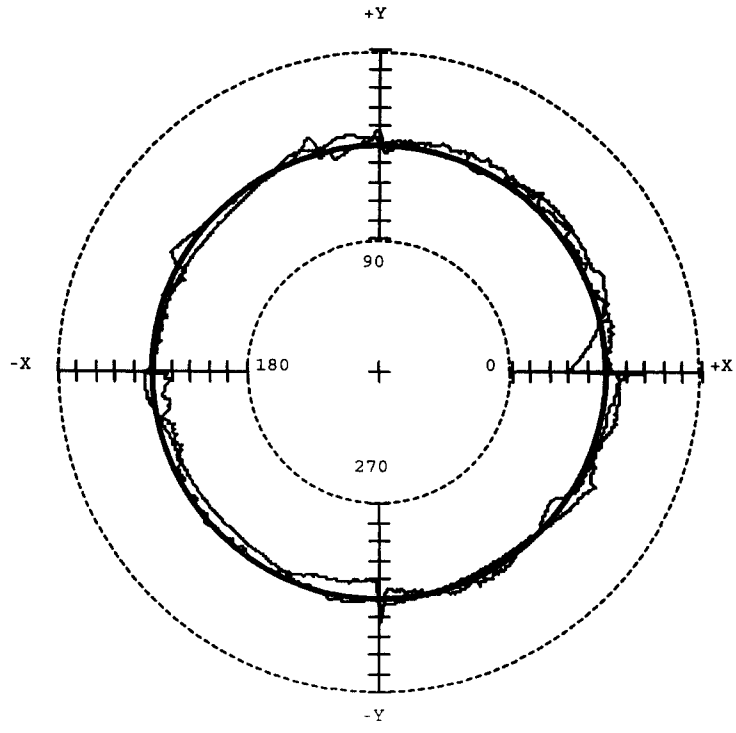

Fig. 16. Differences between the experimental data and the error estimation—two patterns.

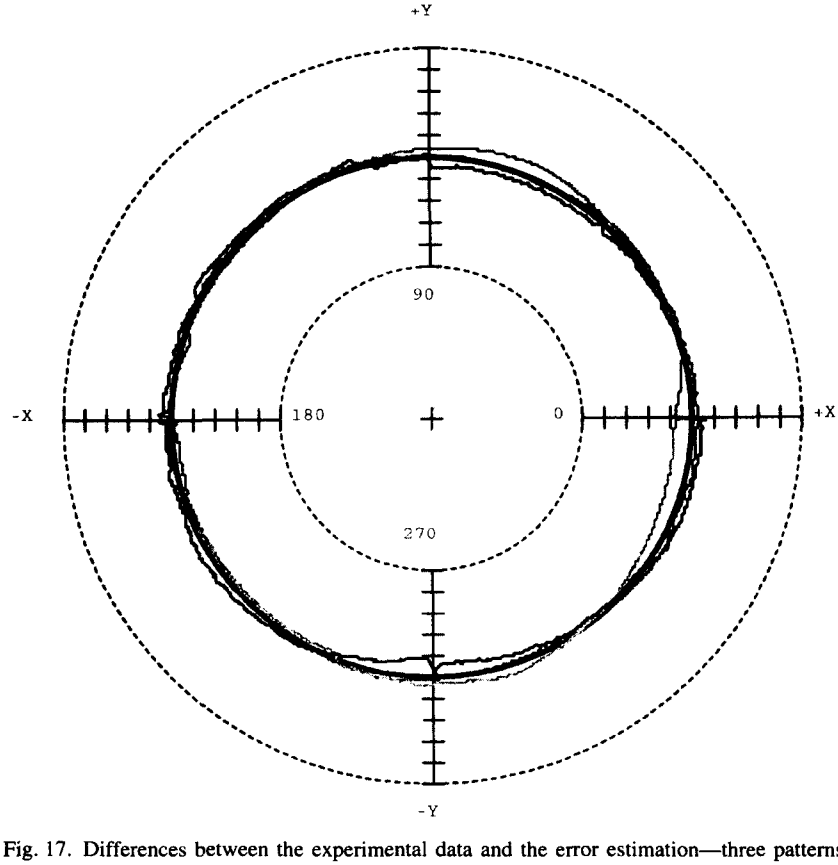

Fig. 17. Differences between the experimental data and the error estimation—three patterns

fied form, such as a first-order (linear), second- or third-order form for guideway systems, whichever is more suitable for a particular use.

From the above diagnosis and analysis, it can be observed that the higher-order model is more complex than the lower-order model in the diagnostic process. On the other hand, the higher-order model is more appropriate for diagnosing higher-precision machines. Therefore, a suitable order model to satisfy the trade-off between precision and complexity to achieve optimal diagnosis is also critical.

Acknowledgements—This research was supported in part by the R.O.C. National Science Council under grant no. NSC 82-0422-E-009-073, and in part by the R.O.C. Industrial Technology Research Institute (ITRI) under grant no. C83028. In addition, the authors would like to thank Mr Chen Yi-Sung, associate researcher at ITRI, and Mr Chang Cheng-Hwei, senior engineer at ITRI, for their enthusiastic assistance and guidance in the experiment- and model-validation testing sessions.

REFERENCES

[1] G.X. Zhang, A Study on the Abbe principle and Abbe error, *Ann. CIRP* **38**(1), 525 (1989).
[2] A.N. Poo, J.G. Bollinger and G.W. Younkin, Dynamic errors in type 1 contouring systems, *IEEE Trans. Ind. Appl.* **8**(4), 477 (1972).
[3] Y. Koren, Cross-coupled biaxial computer control for manufacturing systems, *ASME J. Dyn. Syst. Measmt Control* **102**(4), 265 (1980).
[4] W. Knapp, Test of the three-dimensional uncertainty of machine tools and measuring machines and its relation to the machine errors, *Ann. CIRP* **32**, 459 (1983).
[5] H. Kunzmann, F. Waldele and P.T. Bundesanstalt, On testing coordinate measuring machine (CMM) with kinematic reference standards (KRS), *Ann. CIRP* **32**, 465 (1983).
[6] Y. Kakino, Y. Ihara and Y. Nakatsu, The measurement of motion errors of NC machine tools and diagnosis of their origins by using telescoping magnetic ball bar method, *Ann. CIRP* **36**, 377 (1987).
[7] S.L. Jeng, W.H. Chieng and A.C. Lee, Modeling and diagnosis motion errors of multi-axis machines using a ball bar test, *ASME J. Dyn. Measmt Control* **18**(3), 53 (1996).
[8] J.J. Craig, *Introduction to Robotics Mechanics and Control*. Addison-Wesley, Reading, MA (1986).